Materials Science and Engineering B 121 (2005) 187–191

www.elsevier.com/locate/mseb

Short communication

Grain boundary and grain interior conduction in γ′-Bi_2MoO_6

C.M.C. Vera [a,*], R. Aragón [a,b]

[a] *Laboratorio de Películas Delgadas, Facultad de Ingeniería, Universidad de Buenos Aires, Paseo Colón 850, 1063 Buenos Aires, Argentina*
[b] *CINSO, CONICET, CITEFA, Lasalle 4397, Villa Martelli, Buenos Aires, Argentina*

Received 17 November 2004; received in revised form 24 February 2005; accepted 5 March 2005

Abstract

Impedance spectroscopy of fine grained (<10 μm) γ′-Bi_2MoO_6 samples, in the frequency range of 0.1 Hz–250 kHz, relevant to sensor applications, up to 800 °C, has been used to characterize grain boundary and grain interior contributions to conduction. Above 500 °C, the grain boundary contribution is no longer rate limiting and conduction is dominated by the grain interior component. The corresponding activation energies are 0.98 eV for grain boundary and 0.73 eV for grain interior components. The weak dependence of conductivity on oxygen partial pressure below 500 °C can be attributed to electrode–electrolyte interface phenomena, whereas the robust response to ethanol is commensurate with changes in intrinsic ionic conductivity.

Keywords: Bismuth molybdates; Electrical transport; Conductimetric chemical sensors; Oxygen ionic conduction; Impedance spectroscopy

1. Introduction

The often conflicting requirements for electrical transport properties, depending on their intended application, is reflected by the recent renewed attention paid to oxygen ionic conductors for solid oxide fuel cells, which are electrolytic domain dependent. Pure ionic conduction is desirable for electrolytes and is favored by coarse grain size, which minimizes grain boundary resistance, whereas electrode applications require mixed ionic–electronic character and electronic transport, which is mediated by O_2 exchange with the gaseous phase and consequently benefits from finer textures. In either case, low operating temperature can only be attained at the expense of increased grain boundary resistance.

The point defect structure of γ′-Bi_2MoO_6 mediates high intracrystalline oxygen diffusivity [1,2]. Rapid defect relaxation, in response to changes in the chemical potential of oxygen, promotes substantial variations in bulk resistivity, which have drawn attention to its possible application as a conductimetric sensor for reducing atmospheres [1,3–5]. Ionic conductivity is comparable to that of stabilized zirconia, with the advantage of lower operating temperature. Some disagreement persists on various aspects of electrical transport in this phase, which has alternatively been deemed a pure ionic conductor [6] or a mixed conductor [2,7–12], similarly to other bismuth molybdenum oxides, and motivates the present study on the influence of conduction path, in fine grained ceramics suitable for sensor or catalysis applications.

The use of impedance spectroscopy to characterize grain boundary and grain interior contributions to electrical resistivity, as well as electrode interface phenomena, is well established [13,14] and has been undertaken in this work, in the low frequency range up to 250 kHz, relevant to sensor applications.

2. Experimental

Sintered Bi_2MoO_6 was prepared by solid state reaction of stoichiometric mixtures of reagent grade MoO_3 and Bi_2O_3, ground in an agate mortar, pressed into pellets (9 mm × 3 mm) and heated in air, at 900 °C for 6 h. The procedure was repeated until XRD results were consistent with the high temperature phase γ(H) or γ′-Bi_2MoO_6, by the most

* Corresponding author. Tel.: +54 01143430891x217; fax: +54 01143310129.
E-mail address: cvera@fi.uba.ar (C.M.C. Vera).

0921-5107/$ – see front matter © 2005 Elsevier B.V. All rights reserved.
doi:10.1016/j.mseb.2005.03.006

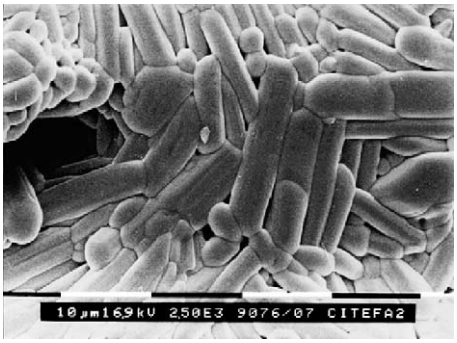

Fig. 1. SEM micrograph of γ'-Bi_2MoO_6, sintered at 900 °C, in air.

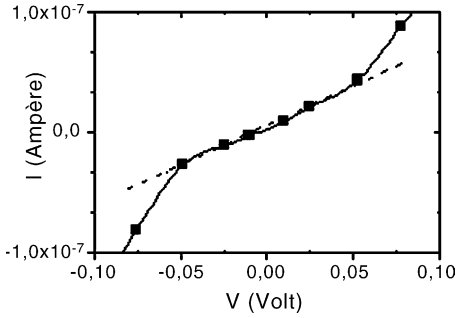

Fig. 2. Potentiostatic DC *I–V* dependence of γ'-Bi_2MoO_6, at 500 °C.

recent convention [15]. SEM (Fig. 1) revealed an average grain size of 10 μm with characteristic prismatic habit. Final density was 83% of the X-ray value (7.85 g/cm^3) [16]. Circular gold electrodes, 100 nm thick with an area of 0.2 cm^2, were deposited by DC magnetron sputtering, on each face of the pellets.

A spring loaded ceramic fixture provided sample support and platinum contacts in pseudo-four-probe configuration, as well as thermometry with a Platinel II thermocouple, in an air tight cylindrical, 24 mm OD sillimanite reactor, placed in a Lindberg Minimite furnace. The fixture was calibrated with standard resistors and capacitors and measurements found consistent with a 1% uncertainty over the range of interest. Controlled atmospheres were ensured by 100 cm^3/min continuous flow of N_2–O_2 mixtures with independent MKS 1179A mass flow controllers. Synthetic air (21% O_2) was adopted as the standard reference.

Complex impedance was measured with an EGG Signal Recovery DSP 7265 lock in amplifier, which resolved the real and imaginary current components, converted to voltage signals by a custom preamplifier, compensated for the bandwidth of interest (0.1 Hz–250 kHz). Potentiostatic DC *I–V* measurements (Fig. 2), at 500 °C, defined the maximum excitation permissible for ohmic behavior, at 50 mV. Isothermal frequency sweeps (0.1 Hz–250 kHz) were undertaken at 50° increments, between 250 and 800 °C. The thermal dependence of DC conductivity (σ) was monitored in the cooling cycle, for this temperature range.

3. Results and discussion

The DC Arrhenius plots (Fig. 3a) are consistent with two distinct regimes. At high temperatures an apparent activation energy of 1.8 eV is in evidence, whereas the corresponding value at low temperatures is 0.8 eV. The gradual change between 400 and 450 °C can be attributed to increased ionic conduction at high temperature, whereas the weak inflexion at 650 °C appears to coincide with the γ''–γ' (or γ(I)–γ(H)) transition [15,17]. Unlike the latter, which is irreversible, the conductivity measurements are reproduced by repeated ther-

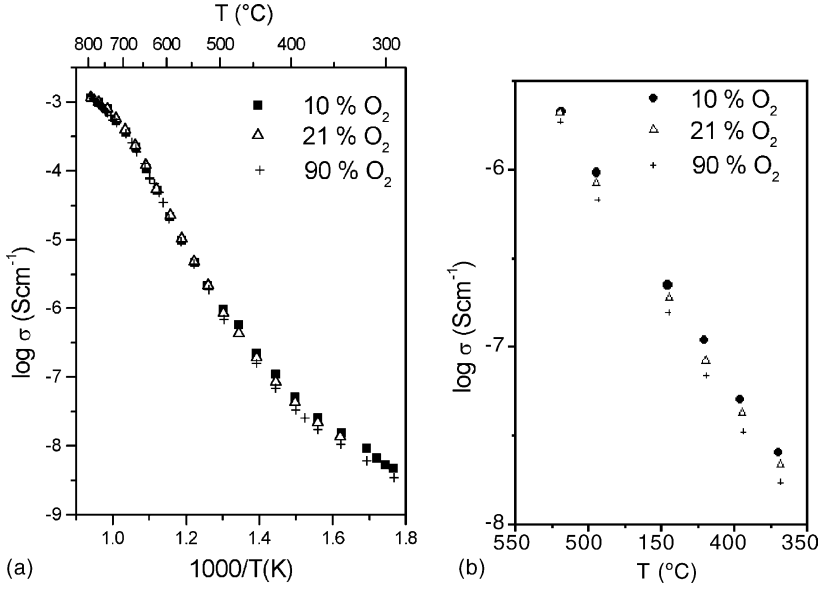

Fig. 3. (a) Two-probe DC-temperature dependence for the conductivity of γ'-Bi_2MoO_6, at different oxygen partial pressures and (b) detail of data (a) below 550 °C.

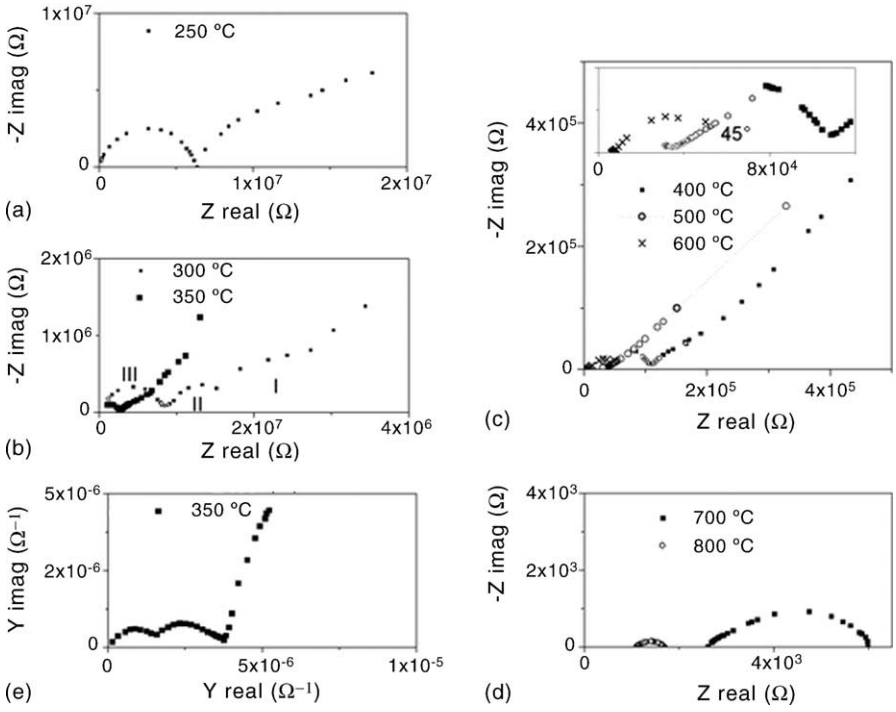

Fig. 4. Impedance spectra of γ′-Bi_2MoO_6 at: (a) 250 °C; (b) 300 and 350 °C; (c) 400, 500 and 600 °C; (d) 700 and 800 °C; (e) admittance plot at 350 °C to improve resolution of Arc II.

mal cycling. DC and fixed frequency thermal scans do not discriminate between the various transport contributions, hence apparent activation energies are dependent on the choice of frequency and of limited physical significance. The absence of potentiostatic control in previous investigations [6,17], to ensure ohmic behavior (Fig. 2), hampers comparison with the present results. The disappearance of the slight dependence on oxygen partial pressure, apparent below 500 °C (Fig. 3b), has been deemed evidence of increased ionic conduction [18]. The influence of p_{O_2} is more readily apparent in extrapolated low frequency measurements which inhibit electrode polarization effects.

Isothermal impedance (Fig. 4) and admittance spectra are consistent with a decrease of the time constants relevant to the conduction processes with increasing temperature, which shifts the corresponding responses to higher frequencies.

Electrode–electrolyte interface phenomena are evidenced by Arc I, whereas grain boundary path conduction is represented by Arc II and grain interior conduction, by Arc III (Fig. 4b) [14,19]. Electrode polarization effects are attenuated by increasing temperature. At 500 °C, the Z_{imag} spike with Z_{real} (Fig. 4c), at a 45° angle, is characteristic of a diffusion controlled Warburg impedance [20,21], which has been attributed in this material [6] to oxygen transport to or from the electrode. The corresponding impedance Arc I is resolved at 700 °C and its extrapolation to the real component axis coincides with the independently measured two probe DC resistance value.

Grain boundary path conduction (Arc II), is clearly resolved at low temperature particularly in the admittance domain [13] of Fig. 4e, and shifts to higher frequency with increasing temperature, consistently with a steeper thermal dependence for grain boundary than for bulk resistance [22]. Above 500 °C, this arc is no longer in evidence, because grain boundary conduction (σ_{gb}) exceeds grain interior conduction (σ_{gi}), hence the real axis intercept reflects intracrystalline resistance. Significantly broadened impedance arcs have been reported [6] at 500 °C, for the low temperature γ-phase, which requires sintering below 600 °C, to avoid transformation to the γ′ polymorph, consistently with a juxtaposed grain boundary conduction arc.

The frequency dependence of the complex impedance was modeled with the equivalent circuit represented in Fig. 5 [13,14,19]. The values of grain boundary resistance (R_{gb}), polarization at grain boundaries (C_{gb}), grain interior resistance (R_{gi}) and grain interior polarization (C_{gi}) could frequently be estimated graphically from the impedance or admittance spectrum. R_{gb}, C_{gb} and C_{gi} were not fitted, whenever the frequency range surveyed proved insufficient. Table 1 summarizes the results for all non-linear least squares fitted parameters [23]. Model spectra for the frequency response of the

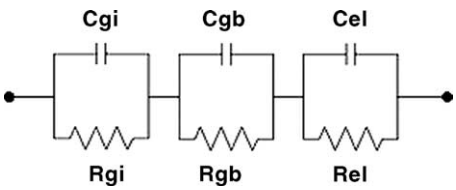

Fig. 5. Model equivalent circuit for non-linear least squares fit.

Table 1
Non-linear least squares [23] fitted parameters for grain boundary and grain interior circuit (Fig. 5) elements

T (K)	R_{gb} (Ω)	C_{gb} (F)	R_{gi} (Ω)	C_{gi} (F)
523	1.4×10^7	8.8×10^{-9}	6.4×10^6	8.5×10^{-13}
573	2.6×10^6	1.0×10^{-9}	8.5×10^5	6.2×10^{-12}
623	6.3×10^5	1.8×10^{-8}	2.6×10^5	3.8×10^{-12}
673	1.4×10^5		1.1×10^5	4.8×10^{-12}
773			1.7×10^4	
873			6.3×10^3	
923			4.0×10^3	
973			2.6×10^3	
1023			1.8×10^3	
1073			1.1×10^3	

equivalent circuit (Fig. 5), calculated with graphically estimated parameters, were consistent with parametric fit results.

Arrhenius plots of σ_{gb} and σ_{gi} (Fig. 6) are linear over the temperature range examined. Above 500 °C, $\sigma_{gb} > \sigma_{gi}$ and the corresponding activation energies are 0.98 eV, for grain boundary, and 0.73 eV, for grain interior conduction, in agreement [22] with the general rule for oxygen ionic conductors. Substantially lower values ($0.5 < E_a < 0.95$) have been reported [6] for coarser grained ceramics, sensitively dependent on sample sintering conditions. The maximum of this range is significantly coincident with the value found for grain boundary conduction.

Below 500 °C, the fixed frequency conductivity of γ′-Bi_2MoO_6, which attenuates the strong electrode polarization phenomena prevalent in DC, is increasingly dependent on the partial pressure of oxygen, which implies some measure of electronic transport, consistent with the mixed character often attributed to this material [2,7–12]. However, impedance spectroscopy at various oxygen partial pressures (Fig. 7) suggests that such behavior is confined to the electrode–electrolyte interface, because the intracrystalline conductivity component remains constant.

Membrane experiments are required [6] to establish the electrolytic domain and modify the pertinent model circuit [24–27], because appreciable electronic conduction would shunt the circuit (Fig. 5) with a parallel resistor [22], which must be independently measured.

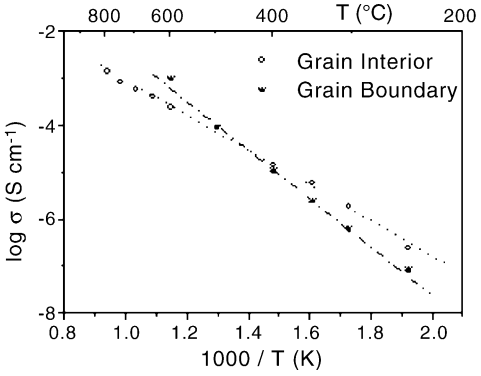

Fig. 6. Thermal dependence of grain boundary and grain interior electrical conductivity in γ′-Bi_2MoO_6.

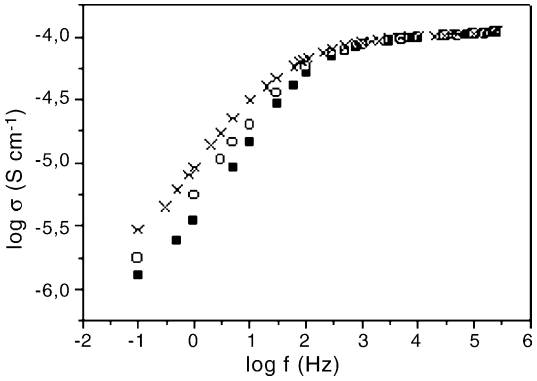

Fig. 7. Logarithmic plot of γ′-Bi_2MoO_6 AC conductivity as a function of frequency, at 500 °C, and p_{O_2} = 1 atm (■); p_{O_2} = 0.32 atm (□); p_{O_2} = 0.1 atm (×).

γ′-Bi_2MoO_6 applications [1,3–5] as a conductimetric sensor for reducing atmospheres rely on the increase of ionic conductivity with oxygen vacancy concentration. For instance, the conductivity change, with a 1.3% by weight of ethanol in N_2 stimulus, at 500 °C (Fig. 8), measured at 10 Hz, in the same pseudo-four-probe configuration used for impedance spectra, is quantitatively consistent with the 47% increase in ionic conductivity observed by impedance spectroscopy (Fig. 9), namely from R_{gi} = 14,273 Ω in N_2, to R_{gi} = 7621 Ω in N_2/ethanol, which corresponds to the low frequency end of Arc III (R_{gi}), and reflects intrinsic bulk properties. Thus, the response to ethanol is qualitatively as well as quantitatively different from the weak low frequency oxygen dependence (Fig. 7), indicative of an electronic contribution to conduction, because the whole effect, regardless of operating frequency, can be accounted by the change in intracrystalline ionic conduction (R_{gi}^{-1}), discriminated by impedance spectroscopy (Fig. 9). This signal is gradually moderated by increasing presence of oxygen in the carrier gas, up to synthetic air, which provides a source of replacement O^{2-} for the created vacancies but, regardless of p_{O_2}, the change upon ethanol injection, as well as the response and relaxation transient, are reproduced by repeated pulsing, as shown in Fig. 8, consistently with the preservation of single solid phase.

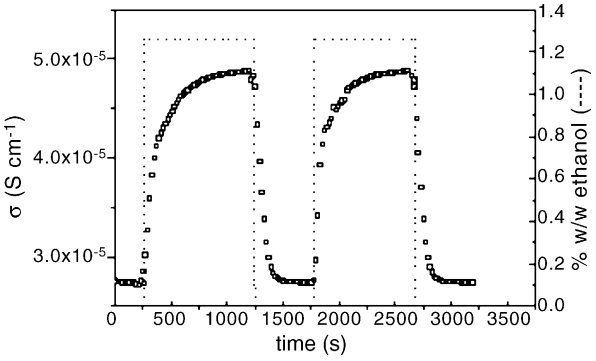

Fig. 8. Electrical conductivity, at 10 Hz, of a γ′-Bi_2MoO_6 pellet, in response to two consecutive 1000 s 1.3% (w/w) ethanol in N_2 (99.999% pure) stimuli.

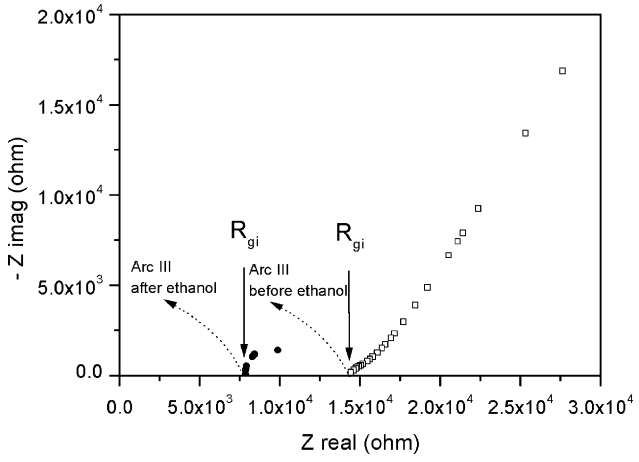

Fig. 9. Impedance spectroscopy of γ'-Bi_2MoO_6, at 500 °C, between 0.1 Hz and 250 kHz, in N_2 (99.999%) atmosphere, before (□) and after (●) injection of 1.3% by weight of ethanol in N_2. R_{gi}, grain interior resistance. Dashed arrows schematically indicate the configuration of Arc III, above 250 kHz.

4. Conclusions

Both inter- and intragranular conduction can be observed below 500 °C, in γ'-Bi_2MoO_6. Above 500 °C, electrical conduction is dominated by the grain interior component. Activation energies for each mechanism were estimated as: 0.98 eV for grain boundary conduction and 0.73 eV, for grain interior conduction. For the fine grained ceramics required by catalysis or sensor applications, the grain boundary mechanism is pertinent.

Whereas the selectivity of γ'-Bi_2MoO_6 resistive chemical sensors ensues from specific surface phenomena, responsible for catalytic activity, the robust and reproducible sensor response can be attributed to dominant bulk ionic conduction, above 500 °C, although mixed ionic–electronic character cannot be excluded, at low temperature. Both regimes are promising for chemical sensing applications, within the respective electrical transport constraints.

References

[1] W.M. Sears, Sens. Actuators B 12 (1993) 95.
[2] H. Iwahara, T. Isaka, T. Sato, T. Takahashi, J. Solid State Chem. 39 (1981) 173.
[3] W.M. Sears, Sens. Actuators 19 (1989) 351.
[4] N. Hykaway, W.M. Sears, R.F. Frindt, S.R. Morrison, Sens. Actuators 15 (1988) 105.
[5] A.R. Raju, C.N.R. Rao, Sens. Actuators B 21 (1994) 23.
[6] L.T. Sim, C.K. Lee, A.R. West, J. Mater. Chem. 12 (2002) 17.
[7] P. Shuk, H.-D. Wiemhöfer, U. Guth, W. Göpel, M. Greenblatt, Solid State Ionics 89 (1996) 179.
[8] L. Boon, R. Metselaar, Solid State Ionics 16 (1985) 201.
[9] L. Boon, R. Metselaar, Eur. J. Solid State Inorg. Chem. 27 (1990) 381.
[10] L. Boon, R. Metselaar, Mater. Sci. Monogr. 28A (1985) 357.
[11] P.J. Gellings, H.J.M. Bouwmeester, Catal. Today 12 (1992) 1.
[12] A. Ziehfreund, W.F. Maier, Chem. Mater. 8 (1996) 2721.
[13] J.E. Bauerle, J. Phys. Chem. Solids 30 (1969) 2657.
[14] J.R. Macdonald, Impedance Spectroscopy, Wiley, New York, 1987.
[15] D.J. Buttrey, T. Vogt, U. Wildgruber, W.R. Robinson, J. Solid State Chem. 111 (1994) 118.
[16] T. Chen, G.S. Smith, J. Solid State Chem. 13 (1975) 288.
[17] D.J. Buttrey, D.A. Jeferson, J.M. Thomas, Philos. Mag. A 53 (1986) 897.
[18] V.I. Utkin, Y.E. Roginskaya, R.P. Kayumov, Y.N. Venevtsev, Zh. Fiz. Khim. 54 (1980) 2953.
[19] S.P.S. Badwal, in: R.W. Cahn, P. Haasen, E.J. Kramer (Eds.), Materials Science and Technology, A Comprehensive Treatment, vol. 11 (vol. editor: M.V. Swain), VCH Verlagsgesellschaft, Weinheim, 1994, pp. 567–633.
[20] P.H. Bottelberghs, in: P. Hagenmuller, W. van Gool (Eds.), Solid Electrolytes, Academic Press, New York, 1978.
[21] A.J. Bard, L.R. Faulkner, Electrochemical Methods, Fundamentals and Applications, 2nd ed., Wiley, 2000.
[22] V.V. Kharton, F.M.B. Marques, E.V. Tsipis, A.P. Viskup, N.P. Vyshatko, M.V. Patrakeev, E.N. Naumovich, J.R. Frade, Solid State Ionics 168 (2004) 137.
[23] J.R. Macdonald, Complex Nonlinear Least Squares Immitance, Inversion and Simulation Fitting Program, LEVM 8.0, 2003.
[24] J. Jamnik, J. Maier, Phys. Chem. Chem. Phys. 3 (2001) 1668.
[25] G.W. Coffey, L.R. Pederson, P.C. Rieke, J. Electrochem. Soc. 150 (2003) 1139.
[26] A. Atkinson, S.A. Baron, N.P. Brandon, J. Electrochem. Soc. 151 (2004) 186.
[27] X. Guo, J. Fleig, J. Maier, Solid State Ionics 154–155 (2002) 563.